# 9

### Research Article

Yawei Ma\*, Jian Wang, Xuyi Peng, and Binxin Si

# Development of a new damping ratio prediction model for recycled aggregate concrete: Incorporating modified admixtures and carbonation effects

https://doi.org/10.1515/rams-2023-0169 received September 04, 2023; accepted December 24, 2023

Abstract: Recycled aggregate concrete (RAC) has been widely used in practical engineering construction. However, the ability of buildings to resist wind-induced vibration and earthquake effects plays an important role in building safety. It is urgent to ensure that recycled concrete still has good antivibration ability within the allowable strength range. By conducting damping tests on recycled concrete specimens, the results show that the damping performance of RAC is better improved compared with natural aggregate concrete. Moreover, the influence of internal factors of recycled aggregates and external environmental conditions on damping performance can be determined, and corresponding damping ratio prediction models can be constructed. However, the current prediction models still have limitations in theory and practice. The existing damping ratio prediction models have a large span of independent variables and do not consider the gradual carbonation effect in the actual environment over time. To overcome these limitations, a new damping ratio prediction model is proposed. Based on the replacement rate of recycled aggregates (RAs) and the amplitude of excitation force, the influence of modified admixtures and carbonation on damping performance is considered, and the corresponding model prediction

formula is constructed. In addition, the influence mechanism is further demonstrated and explained from the macroscopic aspect of specimen profile and the microscopic aspect of electron microscopy tests. It is found that, considering both strength and cost factors, recycled concrete still has good damping performance when the replacement rate of recycled aggregates (RAs) is 40%.

**Keywords:** recycled aggregate concrete, damping performance, prediction model, image processing

# 1 Introduction

Over the past two decades, scholars worldwide conducting extensive research on improving the overall damping performance of structures emerges as a crucial approach to enhance the resilience of civil structures against earth-quakes, wind-induced vibrations, and explosive shocks [1–4]. Recycled aggregate concrete (RAC), as an environmentally friendly and cost-effective building material, has gained increasing attention in structural engineering. Scholars have carried out a lot of research and efforts to improve the mechanical properties of RAC [5–11]. However, there remains ample room for research on its structural performance, particularly in terms of damping properties. Scholars have made some progress [12–14], which offer limited insights into dynamic damping performance during vibration, calling for more profound investigations in this area.

Researchers have explored various factors affecting the damping performance of recycled aggregate (RA) in concrete. One aspect of investigation has been centered around the replacement rate of RA. Jun *et al.* [15–18] found that damping performance was positively correlated with the replacement rate of RA, while Kim *et al.* [6,7,19] conducted a comprehensive survey of relevant tests and reported that the best damping performance occurred between 50 and 100% replacement. Another aspect of the study has focused on

**Jian Wang:** Ministry of Education, Department of Geological Engineering, Lanzhou University, Lanzhou, 730000, China, e-mail: 1142091976@qq.com, wangjian1142@gmail.com

**Xuyi Peng:** Ministry of Education, Department of Geological Engineering, Lanzhou University, Lanzhou, 730000, China,

e-mail: pengxy21@lzu.edu.cn

**Binxin Si:** Ministry of Education, Department of Geological Engineering, Lanzhou University, Lanzhou, 730000, China, e-mail: sibx21@lzu.edu.cn

<sup>\*</sup> Corresponding author: Yawei Ma, Ministry of Education, Department of Geological Engineering, Lanzhou University, Lanzhou, 730000, China; Key Laboratory of Mechanics of Disaster and Environment in Western China, Lanzhou, 730000, China, e-mail: mayw@lzu.edu.cn

particle size. Chaofeng et al. [20,21] observed that in the nonlinear elastic stage, reducing the particle size of recycled coarse aggregate (RCA) increased the damping ratio, and Tianhang [17] also verified the effect of particle size on damping using the free vibration attenuation method. Furthermore, the relationship between damping and excitation frequency in recycled concrete was also investigated by others. Li et al. [22-25] showed a significant correlation, which is, at low excitation frequencies, damping performance was inversely related to frequency, meaning higher frequencies resulted in decreased damping. Pengyuan [26] explained this frequency-dependent behavior from a viscoelastic perspective. Additionally, Zhecheng [27] explored the impact of incorporating modified materials, such as rubber powder and steel fiber, on damping performance, showing gradual improvements with continuous addition. Zhou [28] studied the dynamic modulus of damping ratio by adding polypropylene fiber and air entraining agent. Polypropylene fiber had a positive effect, while air entraining agent had a slight negative impact on mechanical performance. Finally, some scholars [29] investigated the coupling relationship between damping performance and damage development. As excitation force increased, damage gradually increased, but damping performance showed a fluctuating trend, reaching a peak value before gradually decreasing.

Based on the research findings mentioned above, scholars have developed damping prediction models for recycled concrete by considering various factors affecting its damping performance. However, these models exhibit certain limitations: (1) Unequal data spans in the establishment of theoretical models may not accurately reflect the influencing trends, (2) carbonation durability in the actual environment is not considered, and (3) influence factors of modified admixtures are overlooked in model construction. To overcome these limitations, a novel damping ratio prediction model based on a semi-empirical and semi-theoretical approach is proposed in this study. The main contributions can be summarized as follows:

- Analysis of the impact of RA replacement rate and admixture on the damping performance of recycled concrete. Investigation of the influence of RA particle size on damping performance, including its impact trend and mechanism.
- Exploration of the effect of carbonization on the durability of building structures in engineering by examining the damping performance of specimens before and after accelerated carbonization.
- 3) Microscopic validation of the damping effect mechanism. Cube profiles were processed and analyzed through image processing, and microscopic electron microscope tests were conducted on specimens with subsequent image processing analysis of the collected images.

# 2 Experimental test programs

The experimental test program consists of tests executed on RAC cubes and beams that were cast at the Laboratory of the Department of Civil Engineering of Lanzhou University (LZU). In this section, we will first discuss the composition of the different specimens, followed by a description of the accelerated carbonation process, and finally, a report of the set-up of the different monitoring techniques: damping ratio measurements, scanning electron microscope (SEM) test, and image processing.

### 2.1 Test specimens

The study utilized four types of coarse aggregates: natural aggregates (NA5-20) with a size of 5–20 mm, and RCAs (RCA5-20, RCA5-10, and RCA10-20) with different sizes. River sand with a fineness modulus of 2.7 served as the natural fine aggregate. The Chinese standard [30] was followed to determine the physical properties of RCA and natural coarse aggregate (NCA), shown in Table 1. China Cement's P.O 42.5 normal silicate cement specifications and composition are presented in Tables 2 and 3. The modified admixture micron silica and fly ash compositional indices are provided in Tables 4 and 5.

The strength level of specimens is set at C35. Various RAC blends were created by varying replacement rates, particle sizes, and modified admixtures. The ratios and numbers of these blends are listed in Table 6.

### 2.2 Compressive strength experiment

The concrete cubes were cured for 28 days in water at room temperature after being demolded. Referring to the specifications [31] for concrete compressive strength testing, well-cured concrete specimens were carefully selected and

Table 1: Physical properties of the aggregates

| Туре                                   | NCA5-20 | RCA5-20 | RCA5-10 | RCA10-20 |
|--|---------|---------|---------|----------|
| Apparent density/(kg·m <sup>-3</sup> ) | 2,559   | 2,507   | 2,497   | 2,510    |
| Stacking density/(kg·m <sup>-3</sup> ) | 1,377   | 1,251   | 1,367   | 1,219    |
| Moisture content/%                     | 0.4     | 2.17    | 2.31    | 2.02     |
| Water absorption/%                     | 1.05    | 5.47    | 5.79    | 5.07     |
| Crushing index/%                       | 8.7     | 15.2    | _       | 15.3     |

Table 2: Cement properties

| Initial setting | Final setting | Compressive    | Bending        | Burning  | Specific surface area  | Adequacy  |
|-----------------|---------------|----------------|----------------|----------|------------------------|-----------|
| time (min)      | time (min)    | strength (MPa) | strength (MPa) | loss (%) | (m²·kg <sup>-1</sup> ) |           |
| 172             | 234           | 27.2           | 5.5            | 4        | 358                    | Qualified |

Table 3: Chemical component of cement (%)

| CaO   | SiO <sub>2</sub> | Al <sub>2</sub> O <sub>3</sub> | Fe <sub>2</sub> O <sub>3</sub> | MgO  |
|-------|------------------|--------------------------------|--------------------------------|------|
| 53.42 | 24.99            | 5.25                           | 4.81                           | 3.71 |

Table 4: Chemical component of micron silica (%)

| SiO <sub>2</sub> | Al | С   | Са  | Mg  | Cu  |
|------------------|----|-----|-----|-----|-----|
| 95.9             | 1  | 0.9 | 0.1 | 0.2 | 0.2 |

subjected to a predetermined drying period to allow for the evaporation of surface moisture. Subsequently, the compressive test was conducted using a loading rate of 0.5 MPa·s<sup>-1</sup>. The breaking strength was recorded when the specimens exhibited significant deformation. To obtain the final ultimate compressive strength value, the recorded breaking strength was multiplied by a size conversion factor of 0.95.

### 2.3 Accelerated carbonation

To evaluate the damping performance of beam specimens before and after carbonation, in accordance with the specification [32], an accelerated carbonation test of recycled concrete is conducted using a carbonation box. First, the cured test blocks are dried in a drying oven at 60°C for 48 hours. Subsequently, the test blocks are evenly placed inside the carbonation box and subjected to carbonation under standard experimental conditions of  $(70 \pm 5)\%$  relative humidity,  $(20 \pm 2)^{\circ}$ C temperature, and  $(20 \pm 3)\%$  CO<sub>2</sub> concentration.

# 2.4 Measurement of damping ratio

To evaluate the damping performance of beam specimens, the modal analysis method was employed due to its simplicity and the low frequency required for damping measurements [33]. In this study, a new-designed modal method is proposed, in which the beam specimens are suspended by

Table 5: Properties and chemical component of fly ash

| Fineness (5 µm sieve margin %) | Burn vector/% | Al <sub>2</sub> O <sub>3</sub> /% | SiO <sub>2</sub> /% | Moisture content/% | Free CaO/% | Density (g·cm <sup>−1</sup> ) |
|--------------------------------|---------------|-----------------------------------|---------------------|--------------------|------------|-------------------------------|
| 16                             | 2.8           | 24.2                              | 45.1                | 0.85               | 0.85       | 2.55                          |

Table 6: Mix proportions of the concretes

| Туре                         | Α0    | A1   | A2   | A3   | A4   | A5    | A6    | A7    | A9    | A10   |
|------------------------------|-------|------|------|------|------|-------|-------|-------|-------|-------|
| Substitution rate of RCA (%) | 0     | 20   | 40   | 60   | 80   | 100   | 100   | 100   | 100   | 100   |
| Particle size (mm)           | 5-20  | 5-20 | 5-20 | 5-20 | 5-20 | 5-20  | 5–10  | 10-20 | 5-20  | 5-20  |
| Cement (kg)                  | 410   | 410  | 410  | 410  | 410  | 410   | 410   | 410   | 410   | 369   |
| Water (kg)                   | 205   | 205  | 205  | 205  | 205  | 205   | 205   | 205   | 205   | 205   |
| Additional water (kg)        | 0     | 13   | 26   | 38   | 51   | 64    | 64    | 64    | 64    | 64    |
| Sand (kg)                    | 625   | 625  | 625  | 625  | 625  | 625   | 625   | 625   | 625   | 625   |
| NA (kg)                      | 1,160 | 928  | 696  | 464  | 232  | 0     | 0     | 0     | 0     | 0     |
| RCA (kg)                     | 0     | 232  | 464  | 696  | 928  | 1,160 | 1,160 | 1,160 | 1,160 | 1,160 |
| WR (kg)                      | 0     | 0    | 0    | 0    | 0    | 1.84  | 1.84  | 1.84  | 1.84  | 1.84  |
| SiO <sub>2</sub> (kg)        | 0     | 0    | 0    | 0    | 0    | 0     | 0     | 0     | 12.3  | 0     |
| Fly ash (kg)                 | 0     | 0    | 0    | 0    | 0    | 0     | 0     | 0     | 0     | 41    |

Note: WR - Water reducer.

**DE GRUYTER** 

nylon rope to reduce the influence of the support. Various excitation points on the beam specimen were selected for instantaneous hammer excitation, allowing the beam to undergo free decay vibration, as shown in Figure 1. This method offers excellent repeatability, is adaptable to various types of components, and provides accurate results. The displacement amplitude and time curve were recorded using software, and the damping performance of the structure was obtained by analyzing the exponential curve of adjacent amplitudes. During the experiment, a hammer generated an excitation signal to induce free decay vibration in the beam specimen. Sensors received the signal, which was then processed using the dynamic analysis system INV3601 for signal processing. Time-domain measurement was utilized to calculate the damping of the specimen.

For this study, the beam is divided into ten equal parts according to its specific length, and corresponding nodes

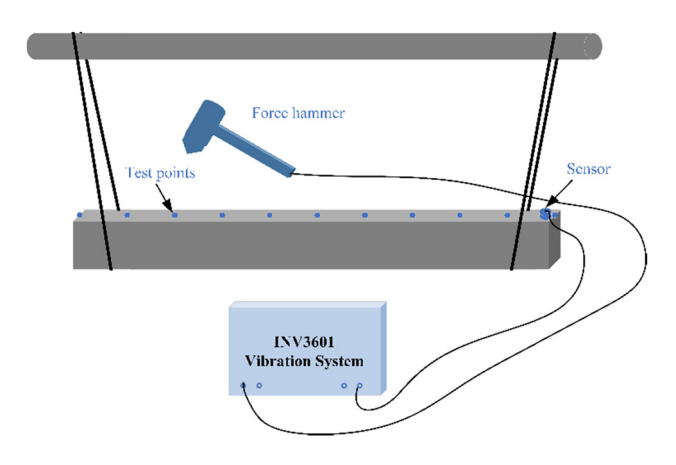
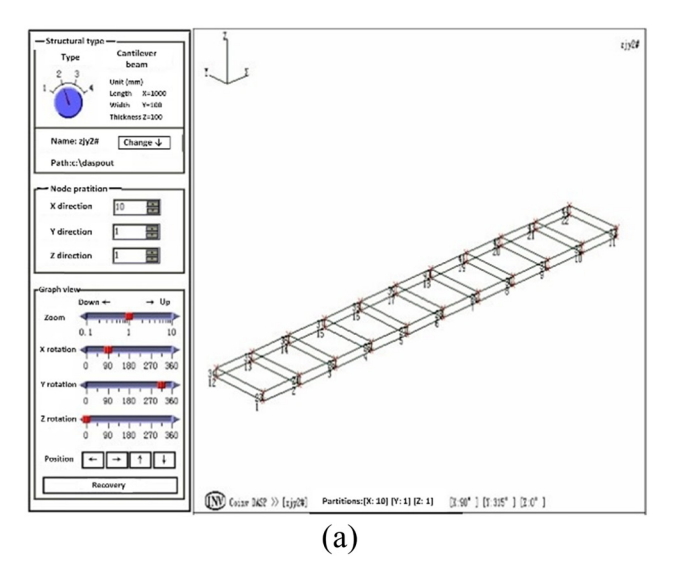


Figure 1: Damping ratio measurement equipment.

are established. Then, modal testing is conducted by sampling the excitation and response signals of the structure, using hammer pulse excitation, and employing either the single-input multiple-output or multiple-input single-output method. The excitation force level is changed as the sensor receives the corresponding signals, and this process is repeated to complete the sampling of all measurement points. The operation interface is depicted in Figure 2.

When using the "triggered sampling" method, the sensor signal undergoes time-domain and the fast Fourier transform (FFT) frequency spectrum analysis. Time-domain analysis is a fundamental signal analysis method, which provides the original time-domain waveform of the signal and plays an important role in various aspects [34,35]. To study the periodicity of a random signal, such as a vibration signal, it is sometimes necessary to transform the signal from the time domain to the frequency domain. The resulting spectrum corresponds to a periodic harmonic component of the signal at each frequency. Time-domain analysis can reveal the amplitude waveform of the signal over time, showing the amplitude at different times and observing changes in signal amplitude over time.

Frequency spectrum analysis is a fundamental signal processing method that finds wide application in various engineering and technical fields [36–38]. Auto-spectrum analysis is a particular method of frequency spectrum analysis that includes amplitude spectrum (PEAK), root mean square (RMS) spectrum, power spectrum, and power spectral density. The amplitude spectrum (PEAK) represents the amplitude of each harmonic component in the frequency domain, while the RMS spectrum represents the effective value amplitude of each harmonic component.



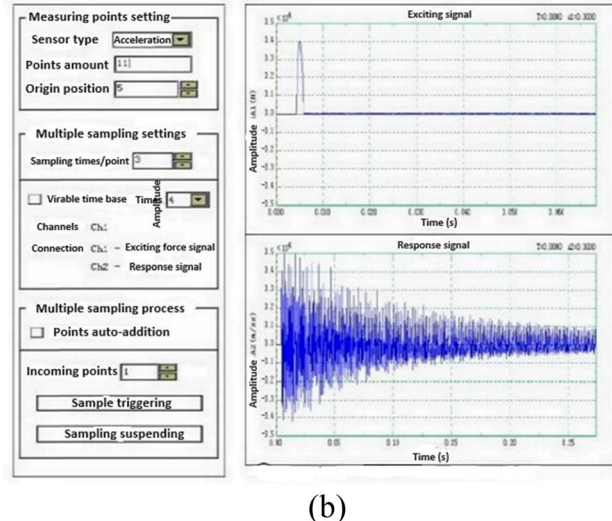


Figure 2: Test data sampling indication. (a) Division of measuring points. (b) Sample data.

The power spectrum indicates the energy or power of each harmonic component, whereas the power spectral density reflects the energy distribution of each harmonic component.

Frequency spectrum analysis typically uses Fourier transform, with the forward transform being:

$$F(\omega) = \int_{-\infty}^{+\infty} f(t)e^{j\omega t} dt.$$
 (1)

Inverse transformation:

$$f(t) = \frac{1}{2\pi} \int_{-\infty}^{+\infty} F(\omega) e^{j\omega t} d\omega.$$
 (2)

Frequency spectrum analysis is a commonly used method for signal analysis, where computers utilize the discrete Fourier transform due to the inability to directly compute continuous Fourier transforms. To improve computational efficiency, the FFT algorithm is commonly employed.

However, during the processing of the signal using FFT, there is a possibility of spectral leakage, which can distort the spectrum. To mitigate this issue, windowing functions are used to reduce spectral leakage. In this study, since the sampled spectrum is a free decay waveform, an exponential window can be applied to improve the signalto-noise ratio, as depicted in Figure 3. After applying the exponential window, data sampling and analysis platform can automatically identify several maximum spectral peaks and display the frequency and amplitude data, thus completing the signal sampling process.

Once all node sampling is complete, modal analysis and calculations can be performed. Frequency domain modal analysis typically involves four steps: transfer function calculation, modal order determination, modal fitting, and mode shape editing.

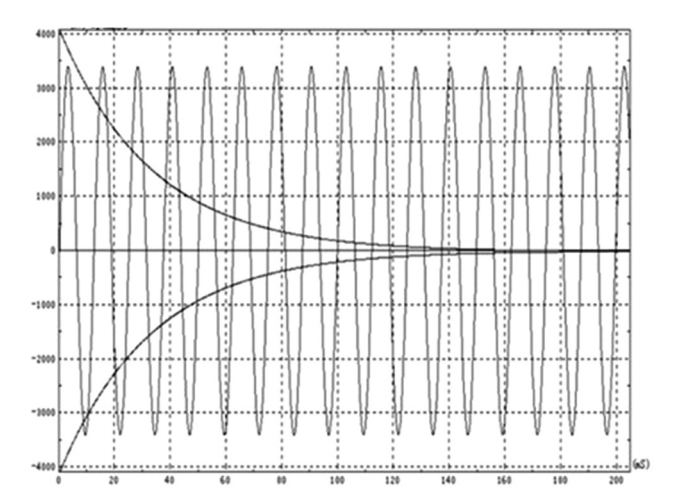


Figure 3: Exponent window function.

Transfer function analysis is a frequency response analysis that reflects the transmission characteristics, such as amplitude-frequency and phase-frequency characteristics, of a system in response to a signal through its input and output signals. This analysis is dependent on the inherent characteristics of the system and is independent of the input signal. The transfer function is defined as

$$H_{XV}(f) = S_V(f)/S_X(f) = P_{XV}(f)/P_{XX}(f).$$
 (3)

where  $H_{xy}(f)$  is the transfer function,  $S_y(f)$  is the FFT of the output signal y(t),  $S_x(f)$  is the FFT of the input signal x (t),  $P_{vv}(f)$  is the cross power spectral density of the output signal, and  $P_{xx}(f)$  is the auto power spectral density of the input signal.

For mechanical systems that only consider single degrees of freedom, dynamic flexibility H can be expressed as follows:

$$H = \frac{x}{F} = \frac{1/K}{1 - (\omega/\omega_n)^2 + j\eta}.$$
 (4)

The absolute value of dynamic flexibility H is

$$|H| = \frac{1/K}{\sqrt{[1 - (\omega/\omega_n)^2]^2 + \eta^2}}.$$
 (5)

There is no doubt that *H* can be defined as a circle with center at  $(0, -1/2K\eta)$  and a diameter of  $1/K\eta$ . The transfer function  $H_{xy}(f)$  obtained can be represented by its real and imaginary components, and its Nyquist plot can be graphed as depicted in Figure 4.

After completing transfer function calculations for all measurement points, modal order determination can be performed. The system can automatically detect peaks and determine the order and corresponding mode. The automatic peak picking method is used to collect the modes corresponding to peak values, and modal order determination is completed after collection.

Following modal order determination, modal fitting can be performed using different methods based on the structural characteristics. In this experiment, the complex mode single degree of freedom fitting method is used. Finally, modal shape editing is necessary to calculate the modal shapes at each order. Here the "mode shape normalization" method is used to process the signals.

Upon completion of modal fitting, the damping can be calculated using the "time-domain analysis" method, specifically the half-power method. When the excitation frequency  $\omega = \omega_n$ , |H| reaches its maximum value,  $|H|_{\text{max}}$ , which is given by

$$|H|_{\text{max}} = 1/K\eta. \tag{6}$$

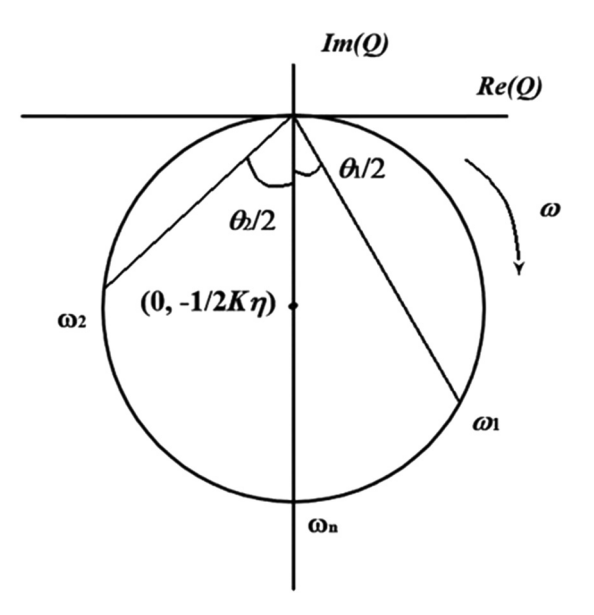


Figure 4: Nyquist plot.

When the reference value of the response  $|H|_{\text{max}}/\sqrt{2}$  is determined, the damping can be calculated based on half-cycle method, which can be expressed as

$$\xi = \frac{\delta}{\sqrt{\pi^2 + \delta^2}}. (7)$$

Thus, the damping ratio can be calculated.

### 2.5 **SEM**

The microstructure of the interface of various recycled aggregate concrete (RAC) specimens before and after carbonation was measured using SEM. The JSM-6710 cold field emission SEM was used as the experimental equipment, as depicted in Figure 5.

### 2.6 Image processing

This chapter highlights the benefits of using image processing technology for studying the cross-sections of cubic blocks and micromorphology of recycled concretes. These advantages encompass efficiency, non-destructiveness, visualization, multiangle observation, and accurate and real-time data acquisition.



Figure 5: JSM-6710 equipment.

Employing image processing technology can enhance research efficiency and accuracy, ensure the integrity and originality of samples, provide more comprehensive information, and improve data accuracy and precision. Additionally, it enables real-time data acquisition and processing, making it an indispensable tool for studying recycled concrete samples.

In this study, Python and OpenCV were employed to process profile images of carbonized specimens, as depicted in Figure 6.

In this study, the contour-processed image was analyzed using area proportion analysis. A grayscale threshold was set for binary conversion, and the area sizes were calculated to obtain the area ratio.

# 3 Results

# 3.1 Compressive strength data

The obtained results are summarized in Table 7.



Figure 6: Image processing flow chart.

Table 7: Summary of compressive strength results

| Туре                 | A0   | A1   | A2   | А3   | A4   | A5   | A6   | A7   | А9   | A10  |
|----------------------|------|------|------|------|------|------|------|------|------|------|
| Compressive strength | 49.8 | 47.6 | 45.9 | 43.5 | 38.3 | 32.1 | 31.7 | 36.1 | 28.9 | 30.8 |

From Table 7, it is evident that the compressive strength of the specimens decreases as the replacement rate of RA increases. This can be attributed to the addition of RA in concrete, which acts as a filler and alters the internal composition of the mixture. Furthermore, the strength of RA itself is generally lower than that of natural aggregate.

Moreover, an increasing trend in compressive strength is observed with the increase in the size of RA. This can be explained by the fact that larger aggregate particles result in reduced internal damage and instability when the specimen

is subjected to pressure. Consequently, fewer and smaller microcracks are formed within the specimen.

Additionally, the use of modified admixtures leads to a decrease in compressive strength. This is evident in test piece A9, where the decrease can be attributed to the high-level water absorption of micro silica powder. During the mortar mixing process, the free water-cement ratio is reduced, affecting the strength of the material. Similarly, in test piece A10, the decrease in strength can be attributed to the mismatch between the high strength grade of cement

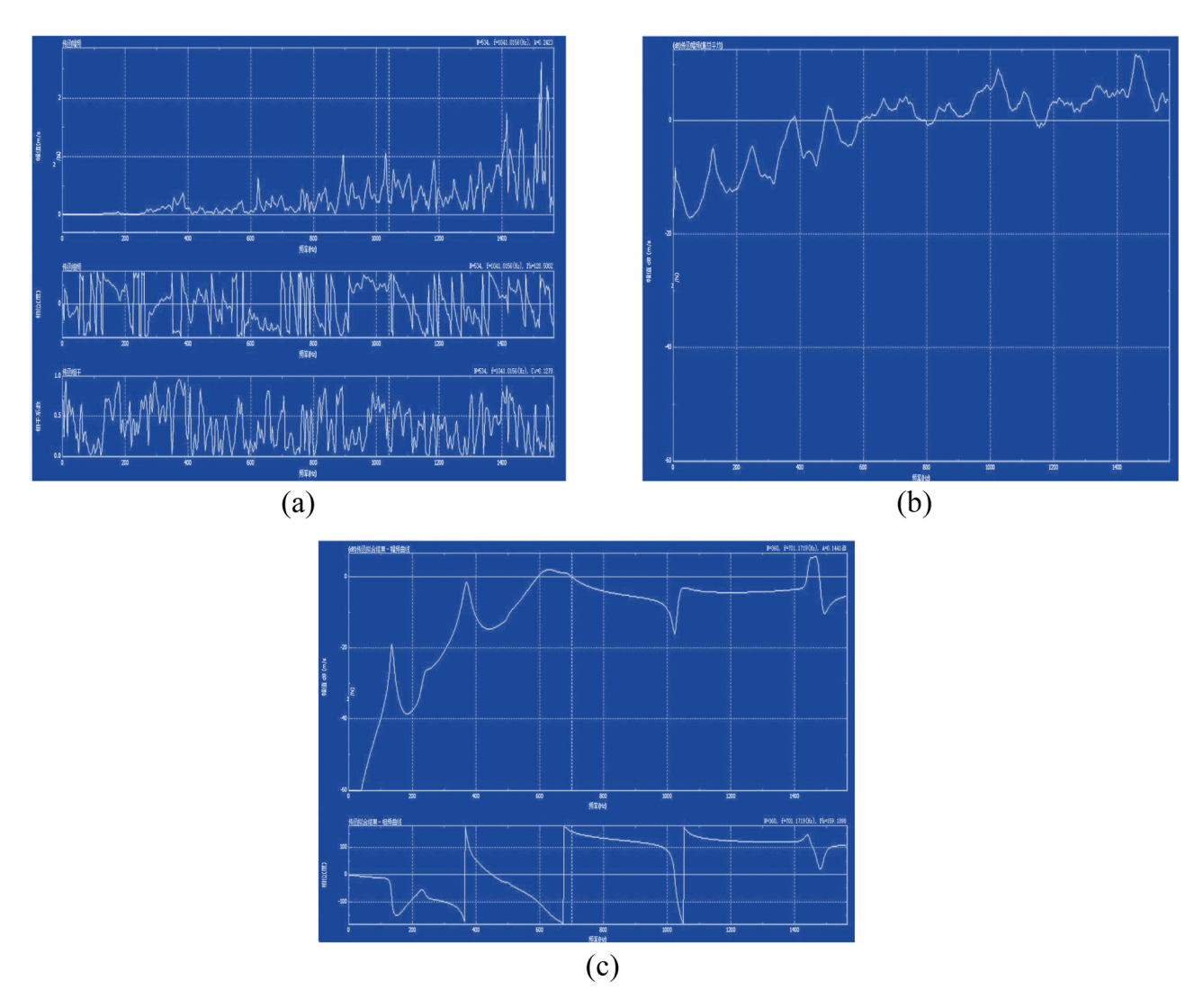


Figure 7: Schematic results of modal analysis. (a) Transfer function calculation. (b) Modal order determination. (c) Modal fitting.

and the activity of the compound fly ash, resulting in a decline in the strength of the composite material.

# 3.2 Damping ratio measurement data

Modal analysis and calculations results can be generated after the damping ratio measurement. Specifically, the modal analysis results can be shown in Figure 7.

When it comes to the calculation of damping ratio, here, the common logarithm is introduced, which is defined as

$$\delta_{10} = \lg \varphi = \delta \lg e = \ln \varphi \lg e.$$
 (8)

Also,

$$\lg e = 0.4343, \, \delta = 2.303\delta_{10}. \tag{9}$$

Therefore, the damping ratio can be calculated using the following formula:

$$\xi = \frac{\lg \varphi}{\sqrt{1.862 + (\lg \varphi)^2}}.$$
 (10)

Since the cantilever beam exhibits multiple modal responses, only the results of the first mode are selected for analysis in this study. High-order mode results are susceptible to interference and may exhibit significant differences. The data collected for the damping ratio calculation are integrated and presented in Table 8.

Based on the results presented in Table 8, an analysis of the relationship between the damping ratio of recycled concrete before and after carbonation and the replacement rate of RA is shown in Figure 8.

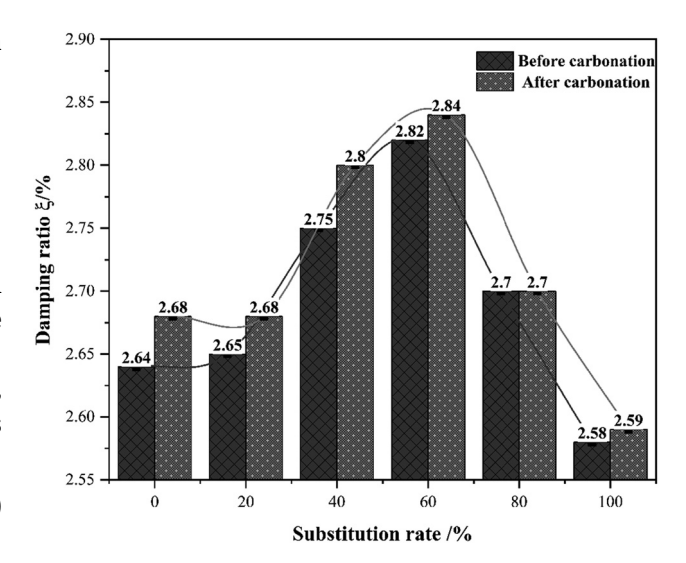


Figure 8: Variation in damping ratio with substitution rate.

The measured damping ratio exhibits a trend of initially increasing and then decreasing as the proportion of RA increases. Specifically, compared to specimen A0 (with no RA), the damping ratios of specimens A1–A4 before carbonation increased by 0.3, 4.1, 6.8, and 2.3%, respectively. After carbonation, this improvement changed to 0, 4.5, 6.0, and 0.07%, respectively. However, the damping ratio of specimen A5 decreased, with reductions of approximately 2.2 and 3.4% before and after carbonation, respectively.

Based on Figure 9, a negative correlation between the damping ratio and the particle size of added RA was observed. Specimen A6 exhibited a 14.2% increase in damping ratio compared to the control group A5, whereas specimen A7 showed a decrease in damping ratio by 12.8%.

Table 8: Damping ratio of specimens under different exciting forces

| Specimen types |           | Damping ratio $\xi$ (%) (before/after carbonation) |           |           |           |  |  |  |
|----------------|-----------|--|-----------|-----------|-----------|--|--|--|
|                | 50 N      | 100 N  | 150 N     | 200 N     |           |  |  |  |
| A0             | 2.57/2.51 | 2.63/2.68  | 2.65/2.70 | 2.72/2.83 | 2.64/2.68 |  |  |  |
| A1             | 2.59/2.63 | 2.62/2.63  | 2.66/2.63 | 2.71/2.81 | 2.65/2.68 |  |  |  |
| A2             | 2.67/2.71 | 2.72/2.70  | 2.76/2.83 | 2.84/2.96 | 2.75/2.80 |  |  |  |
| A3             | 2.73/2.69 | 2.80/2.76  | 2.84/2.85 | 2.92/3.05 | 2.82/2.84 |  |  |  |
| A4             | 2.61/2.66 | 2.67/2.60  | 2.73/2.76 | 2.78/2.77 | 2.70/2.70 |  |  |  |
| A5             | 2.42/2.41 | 2.54/2.61  | 2.63/2.60 | 2.66/2.74 | 2.58/2.59 |  |  |  |
| A6             | 2.74/2.70 | 2.99/2.95  | 3.03/3.13 | 3.05/3.11 | 2.95/2.98 |  |  |  |
| A7             | 2.10/2.20 | 2.15/2.30  | 2.32/2.50 | 2.41/2.51 | 2.25/2.38 |  |  |  |
| A9             | 3.22/3.27 | 3.46/3.55  | 3.65/3.68 | 3.77/3.86 | 3.53/3.59 |  |  |  |
| A10            | 3.28/3.20 | 3.50/3.60  | 3.66/3.71 | 3.76/3.88 | 3.55/3.60 |  |  |  |
| Average        | 2.70/2.69 | 2.81/2.84  | 2.89/2.94 | 2.96/3.05 | _         |  |  |  |

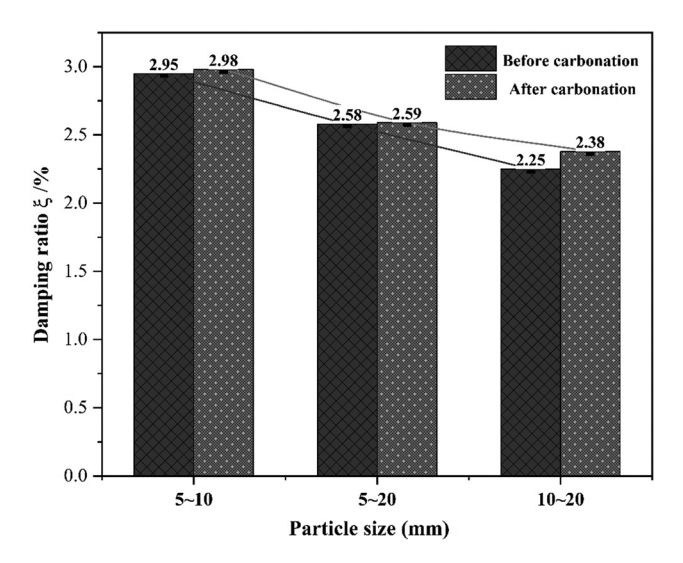


Figure 9: Variation in damping ratio with particle size.

In Figure 10, the relationship between modified additives and the damping ratio of recycled concrete is shown. Concrete specimens A9 and A10, which were added with silica fume and fly ash, respectively, exhibited a significant increase in damping ratio of 36.8 and 37.6% compared to specimen A5.

Upon analysis of the experimental data, a certain linear relationship between the excitation force and damping ratio was observed. The data were then fitted, revealing a favorable linear correlation between the amplitude of the excitation force and the damping ratio of recycled concrete, as depicted in Figure 11. The damping ratio of specimens, both before and after carbonation, increases proportionally with the applied vibration force. This can be attributed to

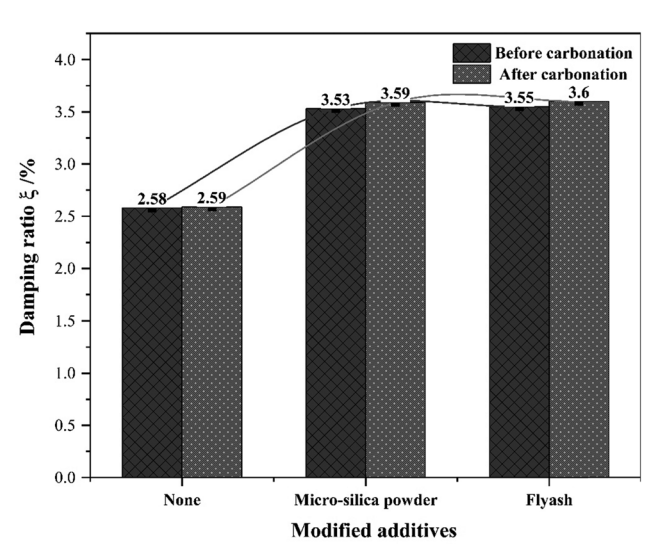


Figure 10: Variation in damping ratio with modified additives.

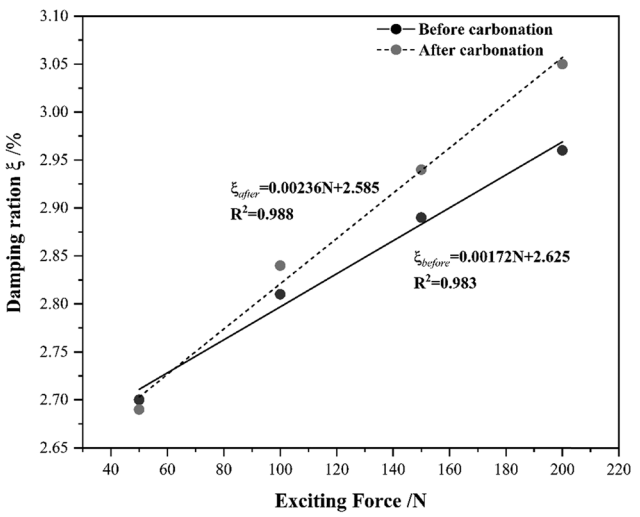


Figure 11: Variation in damping ratio with exciting force.

the gradual increase in internal damage within the recycled concrete component as the load increases, leading to more internal cracks and greater frictional losses. As a result, the interfacial strength between the RCA and the hardened cement mortar decreases, leading to an increase in damping energy consumption.

# 3.3 SEM images

To analyze each influencing factor, specimens A0, A5, A7, and A9 were selected as typical specimens. Electron microscopy was used to scan various RAC specimens. The results are shown in the figures below. The internal morphology of each RAC specimen exhibits significant differences, as illustrated in Figures 12–15.

It is evident that calcium aluminate crystals exhibit needle-shaped objects, C–S–H appears as layered objects, Ca(OH)<sub>2</sub> manifests as clustered deposits, and CaCO<sub>3</sub> appears as blocky objects.

As shown in these figures, SEM images reveal that as the proportion of RAs incorporated into the specimens gradually increases, both the porosity and pore connectivity rise, resulting in a more intricate pore structure. Specifically, within the SEM images, a higher number of voids and pathways between them can be observed, potentially facilitating easier water penetration into the concrete. In terms of aggregate particle size, SEM images show that larger aggregate particles can enhance the mechanical properties of concrete to a certain extent, while correspondingly decreasing its permeability and water absorption, thereby improving its damping performance. In the SEM images, larger gaps between the larger aggregate particles and lower

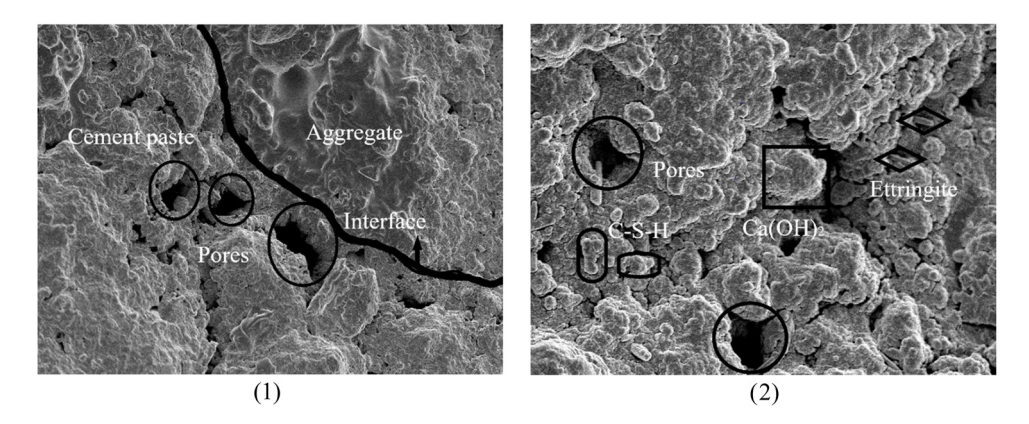


Figure 12: A0 microscopic interface morphology. (1) 1,000 times and (2) 5,000 times.

porosity are noticeable, which could lead to reduced water infiltration and increased concrete damping performance. From the perspective of modified additives, SEM images demonstrate that the addition of modified additives can reduce both porosity and pore connectivity. Specifically, in the SEM images, the particles of modified additives exhibit smoother surfaces, smaller surface areas, and lower porosity, effectively reducing the pore structure.

# 3.4 Images processing outcome

Selecting specimen A0 as a typical example, the result obtained is shown in Figure 16.

We applied grayscale processing to the cross-sectional image using Python. Subsequently, a histogram analysis was conducted on the grayscale image to establish an appropriate threshold for further enhancement. This

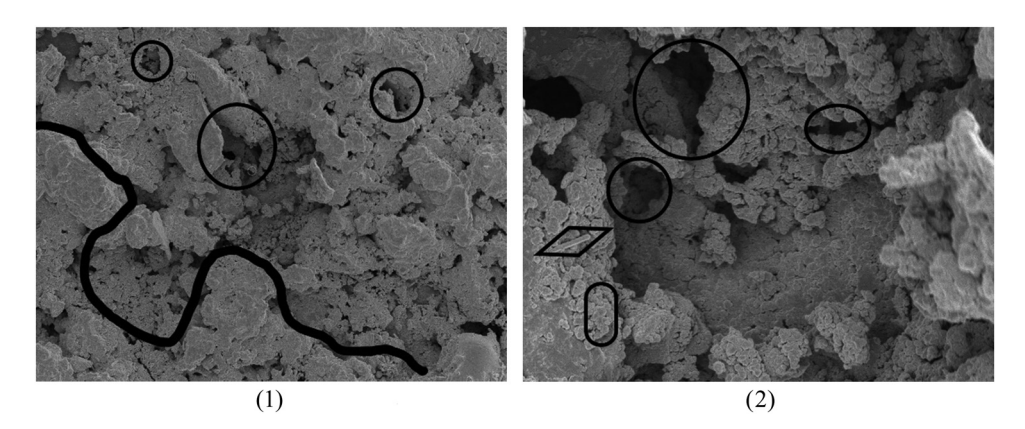


Figure 13: A5 microscopic interface morphology. (1) 1,000 times and (2) 5,000 times.

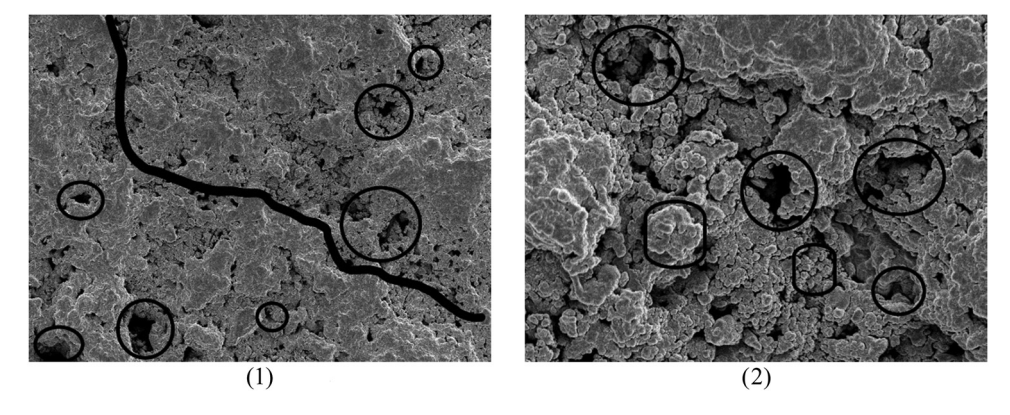
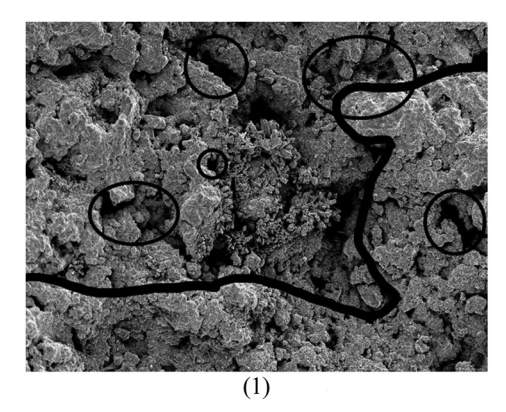


Figure 14: A7 microscopic interface morphology. (1) 1,000 times and (2) 5,000 times.



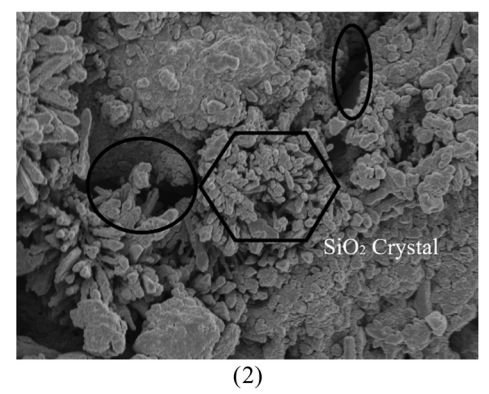


Figure 15: A9 microscopic interface morphology. (1) 1,000 times and (2) 5,000 times.

improved grayscale image was then used for contour detection, representing the edges of particles in the real world. To better determine the proportion of the detected area, we performed noise reduction through filtering operations.

In this study, the contour-processed image was analyzed using area proportion analysis. A grayscale threshold was set for binary conversion, and the area sizes were calculated to obtain the area ratio. The results are presented in Table 9 and Figure 17.

Throughout the carbonation process, there is a noticeable fluctuation in the area proportion occupied by RAs. This fluctuation might be attributed to the partial blockage of existing pores by the by-products of alkaline substances during carbonation. Simultaneously, the ingress of gases into the specimens could lead to gel formation, potentially creating additional pores. However, as the carbonation process progresses towards completion, there appears to be a gradual stabilization in the proportion of pores within the specimens. Regarding the phenomenon discussed earlier, it can be elucidated by considering the mechanisms at play. The initial predominance of RAs, surpassing the 50% mark, followed by a sharp decline to around 51%, is likely due to the interaction between the smaller-sized RAs added and their favorable dispersion characteristics, resulting in a larger surface area. Furthermore, the addition of microsilica to certain specimens, such as A5, A9, and A10, contributes to enhance the homogeneity of the mixture. However, despite this enhancement, it does not significantly augment the area proportion occupied by RAs, particularly at a 100% substitution rate.

Furthermore, Python image processing was employed to analyze the pore area fraction of representative specimens before and after carbonation, which have been shown in Figures 13–16, and the results are presented in Table 10.

When analyzing the data in the table, it becomes evident that porosity increases as the proportion of RAs is augmented. Furthermore, as the particle size of the RAs decreases, porosity exhibits a pronounced increase. However, with the addition of modified admixtures, the internal porosity experiences a certain degree of reduction.

# 4 Discussions

# 4.1 Damping mechanism analysis

The provided data processing results are of paramount importance to our study, as they shed light on the crucial factors influencing the damping performance of the specimens. These factors include the proportion of added RAs, particle size, modified additives, carbonation, and excitation force. In this section, we will delve deeper into the damping mechanism of the specimens and establish a connection between the results and the findings from images processing analysis.

### 4.1.1 Proportion of added RAs

The proportion of added RAs in the specimens appears to play a significant role in their damping performance. As the proportion increases, it is expected that the damping capacity will improve due to the inherent damping properties of the recycled materials [39,40]. However, an excessively high proportion may also lead to reduced interlocking between particles, which could potentially limit the overall damping effectiveness. To gain further insights into changes induced by the varying proportions of RAs, we turned to images processing analysis. SEM analysis revealed that specimens with a moderate proportion of RAs exhibited a well-distributed microstructure, with an

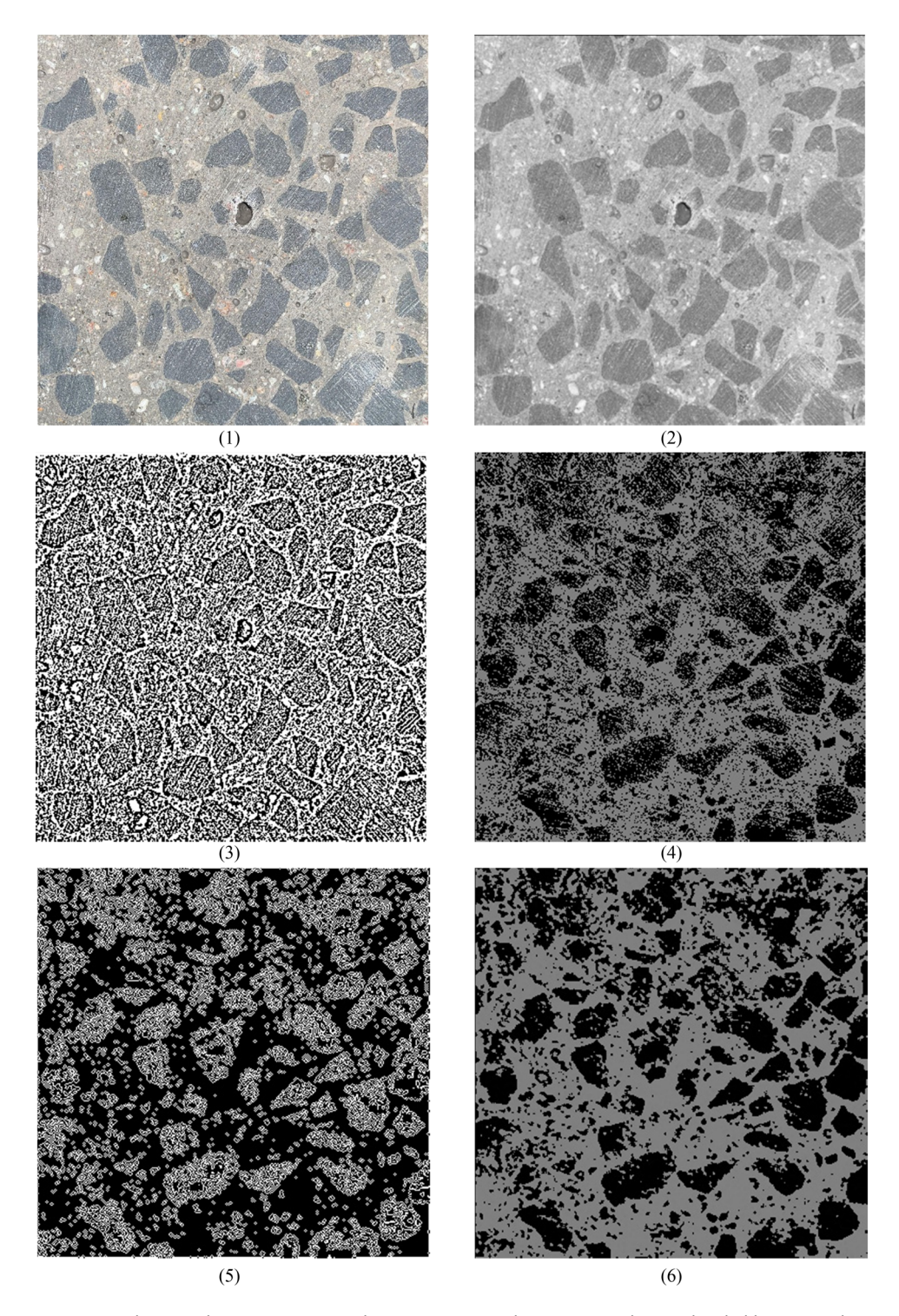


**Figure 16:** Image processing schematic diagram. (1) Section drawing. (2) Grayscale image. (3) Adaptive thresholding. (4) Dichotomy thresholding. (5) Contour processing. (6) Filtering and denoising.

adequate interface between the added aggregates and the matrix material. This favorable interlocking contributes to enhanced energy dissipation and damping capability [41,42]. On the other hand, specimens with an excessive proportion of RAs displayed a less organized microstructure, indicating

poor interfacial bonding and potentially compromising the damping performance. As for the cube profile, when the substitution rate of RAs increases, their dispersion becomes more apparent, resulting in a decrease in the area proportion they occupy, attributed to the larger surface area of the

Table 9: Calculation results of area ratio (%)

| Time    | A0    | A1    | A2    | А3    | A4    | A5    | A6    | A7    | А9    | A10   |
|---------|-------|-------|-------|-------|-------|-------|-------|-------|-------|-------|
| 3       | 57.31 | 50.07 | 49.46 | 47.82 | 47.32 | 49.06 | 49.5  | 49.35 | 54.47 | 53.27 |
| 7       | 45.96 | 52.65 | 53.09 | 52.79 | 50.58 | 53.97 | 54.84 | 59.71 | 58.99 | 49.13 |
| 14      | 43.8  | 57.77 | 58.71 | 55.9  | 57.95 | 57.4  | 57.33 | 55.67 | 54.08 | 41.34 |
| 28      | 56.44 | 54.15 | 46.43 | 52.75 | 52.94 | 57.71 | 59.34 | 53.01 | 48.6  | 45.03 |
| Average | 50.87 | 53.66 | 51.92 | 52.31 | 52.19 | 54.53 | 55.25 | 54.43 | 54.03 | 47.19 |

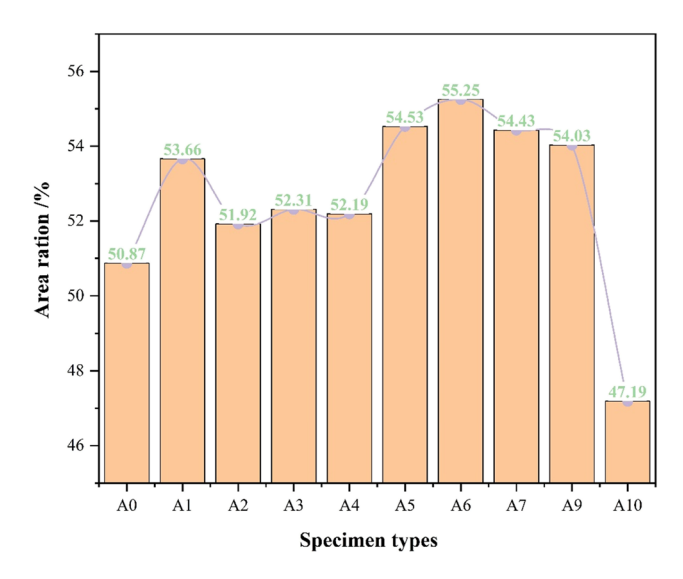


Figure 17: Section area ratio of specimen.

RAs with old cement mortar compared to natural aggregates. However, the overall area proportion does not decrease compared to the initial value.

### 4.1.2 Particle size

Particle size is another crucial parameter affecting the damping behavior of the specimens [43,44]. Generally, larger particles tend to provide more energy dissipation due to increased friction and sliding at the particle interfaces. However, finer particles may contribute to better packing and improved load transfer within the material, resulting in enhanced damping. SEM examination of specimens with varying particle sizes corroborated these assumptions. Specimens with larger particle sizes exhibited rougher surfaces. promoting more frictional interactions [45,46]. In contrast, specimens with smaller particles displayed a denser arrangement and a smoother surface, which likely facilitated more effective load transfer and, consequently, better damping performance. Moreover, when smaller-sized RAs are added, their area proportion is relatively high due to their good dispersion and large surface area.

Table 10: Calculation results of pore area proportion (%)

| Items | Ratio (%) |
|-------|-----------|
| A0    | 5.38      |
| A5    | 7.42      |
| A7    | 13.57     |
| A9    | 4.84      |

### 4.1.3 Modified additives

The introduction of modified additives can significantly alter the damping properties of the specimens. The nature of these additives, such as rubber or other damping agents, can lead to enhanced viscoelastic behavior, which plays a vital role in damping vibrations and dissipating energy [43,46]. SEM investigations of specimens with modified additives demonstrated a noticeable difference in microstructure compared to the control samples. The presence of these additives contributed to the formation of damping domains within the material, where energy dissipation was concentrated. This phenomenon highlights the effectiveness of modified additives in enhancing the damping capacity of the specimens. The addition of micro-silica to specimens A5, A9, and A10 improves the mixture's homogeneity but does not significantly increase the area proportion of RAs, particularly at a 100% substitution rate. In contrast, the addition of fly ash has a significant effect on the dispersion of RAs, resulting in a significant reduction in the area proportion occupied by aggregates, as fly ash has better particle size and dispersion properties compared to Portland cement.

### 4.1.4 Carbonation

The damping ratio shows minimal fluctuations and only a slight reduction between the pre-carbonation and post-carbonation states. The minor reduction in damping ratio between the pre-carbonation and post-carbonation states can be attributed to several factors [47-49]. First, the carbonation process may lead to the formation of calcium

**Table 11:**  $k_m$  values of different modified admixtures

| Types | Rubber    | Rubber fiber | Steel fiber | Fly ash   | Micro-silica powder |
|-------|-----------|--------------|-------------|-----------|---------------------|
| Range | 1.07~1.59 | 1.45~2.79    | 1.06~1.15   | 1.29~1.36 | 1.26~1.38           |

Table 12: Function fitting data results

| Types  | а      | b                          | с                         | D                         | Reduced Chi-Square |
|--------|--------|----------------------------|---------------------------|---------------------------|--------------------|
| Values | 1.0005 | -1.3704 × 10 <sup>-4</sup> | 1.1025 × 10 <sup>-6</sup> | 2.7453 × 10 <sup>-4</sup> | 0.00881            |
| Error  | 0.110  | $2.1746 \times 10^{-5}$    | 2.9710 × 10 <sup>-7</sup> | 1.9558 × 10 <sup>-4</sup> | _                  |

carbonate within the concrete matrix. This can result in a denser and more compacted microstructure, which may slightly increase the stiffness of the material and lead to a small decrease in the damping ratio. Second, carbonation can alter the pore structure of the concrete, affecting the internal energy dissipation mechanisms. Changes in the porosity and pore size distribution may influence the damping behavior of the material, contributing to the observed slight reduction in damping ratio.

ence the damping performance of the specimens. SEM analysis provides valuable insights into the microstructural changes associated with these factors, allowing for a better understanding of the damping behavior and paving the way for the development of advanced damping materials with enhanced performance for various engineering applications.

modified additives, and excitation force all significantly influ-

### 4.1.5 Excitation force

The excitation force applied to the specimens during testing can influence their damping performance [24,25]. Higher excitation forces may lead to more pronounced vibrations, necessitating greater damping capacities to absorb and dissipate the excess energy.

In conclusion, the comprehensive analysis of the damping mechanism reveals that the proportion of RAs, particle size,

# 4.2 Damping model construction

Based on the previous analysis, it is assumed that the damping ratio is a linear function of the excitation force and a quadratic function of the displacement rate, without any coupling effect between these two variables. As the selected aggregate particle size cannot be uniform in a specific range and is not considered, a modification parameter  $k_m$  is introduced. Therefore, in this study, the damping ratio can be expressed using the newly created formula.

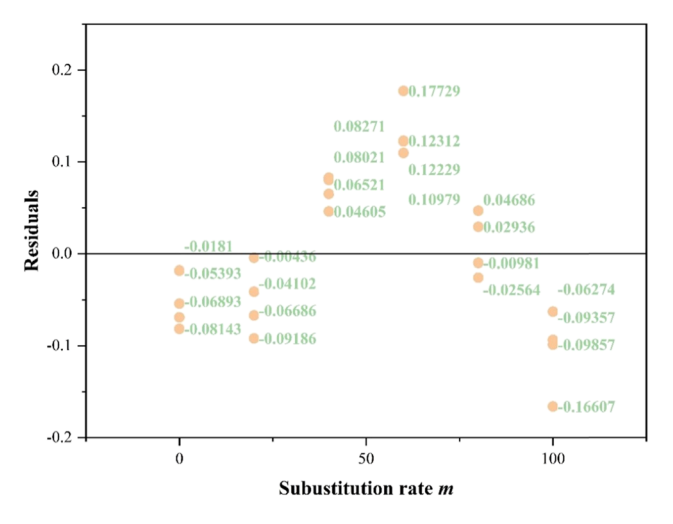


Figure 18: Residual of independent variable m.

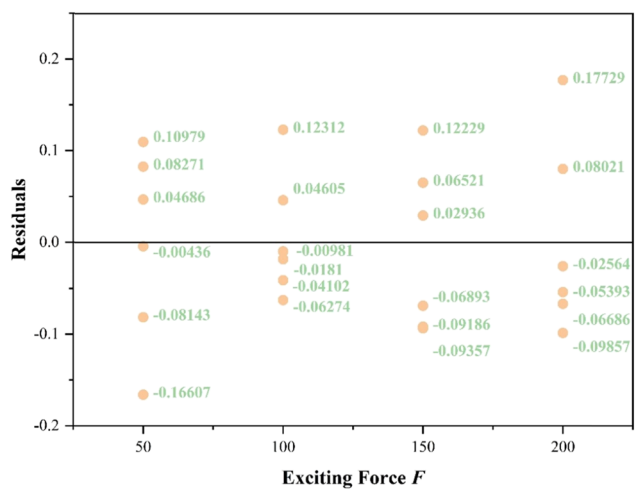


Figure 19: Residual of independent variable F.

$$\xi = k_0 k_m (a + bF + cm^2 + dm), \tag{11}$$

where  $k_m$  represents modification coefficient, with  $k_m = 1$ when there is no addition. When there is an addition, the specific values of  $k_m$  can be found in Table 11 based on relevant literature [50-53]. The values will vary slightly in a small range depending on various sources of raw material, and for damping ratio calculation the selected value with permissible limits will be suitable. *m* represents the replacement rate, and F represents the excitation force,  $k_0$  is defined here as the characteristic damping of the original RA, which depends only on the source of the RA.

The values of each coefficient can be obtained by fitting the data in Table 12, as shown in Figures 18 and 19.

Based on the excellent data fitting results shown in Table 11, we can conclude that the residual values are very small, both in phase and in parameter errors. To further illustrate the goodness of fit for each parameter, we have visualized the residual values for m and F. As depicted in the Figures 18 and 19, the residual values for both parameters are exceptionally small.

Therefore, the following formula can be obtained:

$$\xi = k_0 k_m (1 - 1.37 \times 10^{-4} F + 1.10 \times 10^{-6} \text{m}^2 + 2.74 \times 10^{-4} \text{m}),$$
(12)

where  $k_m$  can be decided via Table 11, while  $k_0$  is 2.58 due to this experiment.

# 5 Summary, conclusion, and future works

The conclusion of this work presents a comprehensive study of the damping performance of recycled concrete beams using modal analysis. The research investigates the influence of various factors on the damping performance of recycled concrete beams and establishes an accurate damping ratio prediction model. The model takes into account the effects of modified admixtures, substitution ratios, and excitation forces on the damping performance of specimens. Additionally, through image processing of cubic profile samples and microscopic electron microscopy experiments, the damping mechanism of recycled concrete is thoroughly understood from both macroscopic and microscopic perspectives.

Taking into consideration that when the replacement rate of RAs is below 60%, the compressive strength of recycled concrete experiences only a slight decline, which does not adversely affect its practical usability. Moreover, in the range of 40-60% replacement, the concrete's damping properties show a significant improvement. However, as the replacement rate of RAs increases, the cost of concrete steadily rises. Considering a comprehensive evaluation of factors including strength, damping performance, and cost, the optimal replacement rate for RAs is determined to be 40%. Also, the damping ratio prediction model can be summarized as  $\xi = k_0 k_m (1 - 1.37 \times 10^{-4} F + 1.10 \times 10^{-6} m^2 + 2.74 \times 10^{-4} m).$ 

However, it is important to acknowledge the limitations of the damping ratio experiments, particularly under conditions of significant deformation. Additionally, to enhance the model's applicability, further improvements can be made to the model considering the variation in modified admixture parameters found in different literature sources. Ensuring consistency in experimental results will necessitate enhancing the generality of the model. Future research should aim to address these issues to advance the field of study.

**Acknowledgments:** The authors are thankful for the support by the National Natural Science Foundation of China (No. 52278184).

Funding information: The work here was supported by the National Natural Science Foundation of China (No. 52278184).

**Author contributions:** All authors have accepted responsibility for the entire content of this manuscript and approved its submission.

**Conflict of interest:** The authors state no conflict of interest.

Data availability statement: The datasets generated and/ or analysed during the current study are available from the corresponding author on reasonable request.

### References

- Bruschi, E. and V. Quaglini. Reliability analysis of two archetype RC buildings with hysteretic dampers. Soil Dynamics and Earthquake Engineering, Vol. 176, 2024, id. 108290.
- Reynolds, P., M. J. Wesolowsky, E. J. Hudson, A. Pavic, S. Rahman. [2] Practical application of active mass damping for floors in a commercial building. In Conference Proceedings of the Society for Experimental Mechanics Series, 2024, pp. 191-197.
- [3] Terenzi, G., E. Fuso, and S. Sorace. Structural performance study and improvement of artemio franchi stadium in florence. Engineering Structures, Vol. 298, 2024, id. 117068.
- Wu, D., B. Zhao, and H. Zhu. Experimental study on effect of [4] assembly process on seismic performance of modular precast composite shear wall structures. Journal of Building Engineering, Vol. 80, 2023, id. 107916.
- Zhang, H., J. Xiao, Y. Tang, Z. Duan, and C.-S. Poon. Long-term shrinkage and mechanical properties of fully recycled aggregate

- concrete: Testing and modelling. *Cement & Concrete Composites*, Vol. 130, 2022, id. 104527.
- [6] Wang, B., L. Yan, Q. Fu, and B. Kasal. A comprehensive review on recycled aggregate and recycled aggregate concrete. *Resources Conservation and Recycling*, Vol. 171, 2021, id. 105565.
- [7] Kim, J. Influence of quality of recycled aggregates on the mechanical properties of recycled aggregate concretes: An overview. Construction and Building Materials, Vol. 328, 2022, id. 127071.
- [8] Ashraf, M. J., M. Idrees, and A. Akbar. Performance of silica fume slurry treated recycled aggregate concrete reinforced with carbon fibers. *Journal of Building Engineering*, Vol. 66, 2023, id. 105892.
- [9] Tang, Y. C., Y. F. Wang, D. X. Wu, Z. H. Liu, H. X. Zhang, M. Zhu, et al. Exploring temperature-resilient recycled aggregate concrete with waste rubber: An experimental and multi-objective optimization analysis. *Reviews on Advanced Materials Science*, Vol. 62, 2023, id. 20230347.
- [10] Chen, Z., J. Yu, Y. Nong, Y. Yang, H. Zhang, and Y. Tang. Beyond time: enhancing corrosion resistance of geopolymer concrete and BFRP bars in seawater. *Composite Structures*, Vol. 322, 2023, id. 117439.
- [11] Tang, Y., et al. An experimental investigation and machine learning-based prediction for seismic performance of steel tubular column filled with recycled aggregate concrete. *Reviews on Advanced Materials Science*, Vol. 61, 2022, pp. 849–872.
- [12] Liang, C., Y. Fu, C. Wang, Y. Gao, and J. Zhao. Damping of rubberized recycled aggregate concrete and damping estimation of its elements by finite element analysis. *Composite Structures*, Vol. 281, 2022, id. 114967.
- [13] Li, T., J. Xiao, T. Sui, C. Liang, and L. Li. Effect of recycled coarse aggregate to damping variation of concrete. *Construction and Building Materials*, Vol. 178, 2018, pp. 445–452.
- [14] Li, T. and J. Xiao. The damping property of damaged recycled aggregate concrete after loading. *Journal of Building Engineering*, Vol. 35, 2021, id. 102096.
- [15] Jun, M., C. Yang, and L. Ping. Experimental study on the performance of large deformation damping aggregate concrete regeneration. *Value Engineering*, Vol. 34, 2015, pp. 129–130.
- [16] Chaofeng, L., L. Tiejun, X. Jianzhuang, and Z. Dujian. Experimental study on relationship between damping capacity and damage degree of recycled concrete cantilever beam. *China Civil Engineering Journal*, Vol. 49, 2016, pp. 100–106.
- [17] Tianhang, B. Reseach on damping property of recycled aggregate concrete. Thesis. Harbin Institute of Technology, 2012.
- [18] Jianzhuang, X., X. Hao, and L. Yun. Damping properties of recycled aggregate concrete and simply-supported recycled aggregate concrete slabs. *Journal of Tongji University (Natural Science)*, Vol. 48, 2020, pp. 498–505.
- [19] Strukar, K., T. K. Sipos, I. Milicevic, and R. Busic. Potential use of rubber as aggregate in structural reinforced concrete element - A review. *Engineering Structures*, Vol. 188, 2019, pp. 452–468.
- [20] Chaofeng, L., H. Jiajun, X. Jianzhuang, and L. Yun. Damping property and mechanism of recycled aggregate concrete beams. *Journal of Tongji University (Natural Science)*, Vol. 46, 2018, pp. 737–743 + 750.
- [21] Chaofeng, L., L. Tiejun, Z. Dujian, Y. Qiuwei, and F. Li. Damping capacity of recycled concrete. *Journal of Vibration and Shock*, Vol. 32, 2013, pp. 160–164.
- [22] Li, T., J. Xiao, T. Sui, C. Liang, and L. Li. Effect of recycled coarse aggregate to damping variation of concrete. *Construction and Building Materials*, Vol. 178, 2018, pp. 445–452.

- [23] Chaofeng, L., X. Jianzhuang, W. Chunhui, M. Zhiming, and H. Zhihai. Frequency-dependent damping properties of recycled aggregate concrete. *Journal of Materials in Civil Engineering*, Vol. 33, 2021, id. 04021160.
- [24] Yifan, F., T. Yuan, H. Yuli, and L. Xinzheng. Influence of damping models on dynamic analyses of a base-isolated composite structure under earthquakes and environment vibrations. *Engineering Mechanics*, Vol. 39, 2022, pp. 201–211.
- [25] Li, T., J. Xiao, and A. Singh. Influence of new-to-old concrete interface on the damping behavior of recycled aggregate concrete. Structural Concrete, Vol. 22, 2021, pp. 3109–3122.
- [26] Pengyuan, Z., W. Yuanfeng, L. Baodong, G. Kun, and X. Jianzhuang. Rate-dependent damping properties of recycled aggregate concrete from creep perspective. *Construction and Building Materials*, Vol. 273, 2020, id. 121691.
- [27] Zhecheng, L. Experimental study on mechanical and damping properties of modified recycled concrete. Master. Nanchan University, 2018.
- [28] Zhou, C., X. Pei, W. Li, and Y. Liu. Mechanical and damping properties of recycled aggregate concrete modified with air-entraining agent and polypropylene fiber. *Materials*, Vol. 13, 2020, id. 2004.
- [29] Jun, M. Research on damping property of recycled aggregate concretes. Master. Yangzhou University, 2015.
- [30] "Standard for technical requirements and test methods of sand and crushed stone (or gravel) for ordinary concrete," vol. JGJ 52-2006, ed, 2006.
- [31] "Standard for test method of mechanical properties on ordinary concrete" vol. GB/T50081-2002, ed: China Academy of Building Research, 2002.
- [32] "Standard for test method of long-term performance and durability of ordinary concrete," vol. GB/T 50082-2009, ed: China Academy of Building Research, 176P.; B5, 2009.
- [33] Sugapriya, P., R. Ramkrishnan, G. Keerthana, S. Saravanamurugan. Experimental investigation on damping property of coarse aggregate replaced rubber concrete. In *International Conference on Advances in Materials and Manufacturing Applications (IConAMMA)*, Bengaluru, INDIA, 2017, Vol. 310, id. 012003, 2018.
- [34] Yu, X., D. Dan, and L. Ge. Time-domain distributed modal parameter identification based on mode decomposition of single-channel vibration response. *Engineering Structures*, Vol. 289, 2023, id. 116323.
- [35] Yu, X. and D. Dan. Structural modal parameter identification based on 2D spectral analysis. *Journal of Sound and Vibration*, Vol. 552, 2023, id. 117638.
- [36] Ke, X., et al. The nth power Fourier spectrum analysis for the generalized seismic wavelets. *IEEE Transactions on Geoscience and Remote Sensing*, Vol. 61, 2023, id. 5904010.
- [37] Hou, C., G. Liu, Q. Tian, Z. Zhou, L. Hua, and Y. Lin. Multisignal modulation classification using sliding window detection and complex convolutional network in frequency domain. *IEEE Internet* of *Things Journal*, Vol. 9, 2022, pp. 19438–19449.
- [38] Golyandina, N. and A. Korobeynikov. Basic singular spectrum analysis and forecasting with R. Computational Statistics & Data Analysis, Vol. 71, 2014, pp. 934–954.
- [39] Banghu, J. and G. Ying. Research on damping properties of recycled concrete. *Journal of Hubei University of Education*, Vol. 35, 2018, pp. 16–18.
- [40] Jinxi, Z., Z. Jianhua, and W. U. Changsen. Study on properties and pore structure of recycled concrete. *Journal of building materials*, Vol. 9, 2006, pp. 142–147.

- [41] Guojun, K., D. Ming, P. Hong, and C. Zhenfu. Damping ratio of concrete after its coarse aggregate surface is treated by viscoelastic materials. Journal of Building Materials, Vol. 12, 2009, pp. 605-608.
- [42] Wengui, L., X. Jianzhuang, and Y. Junqiang. Stress distribution characteristics of modeled recycled aggregate concrete under uniaxial compression. Journal of Tongji University(Natural Science), Vol. 40, 2012, pp. 906-913.
- [43] Zhang, X., X. Kuang, H. Niu, and J. Yang. Research progress on material properties of recycled aggregate concrete modified by waste rubber. Bulletin of the Chinese Ceramic Society, Vol. 36, 2017, pp. 4050-4059.
- [44] Wang, R., Y. Zhao, Y. Gou, and P. Xu. Experimental study on stressstrain relationship of recycled coarse aggregate concrete with different particle size under uniaxial compression. Water Resources and Hydropower Engineering, Vol. 49, 2018, pp. 193-198.
- [45] Wang, D., et al. Mechanical performance of recycled aggregate concrete in green civil engineering: Review. Case Studies in Construction Materials, Vol. 19, 2023, id. E02384.
- [46] Pedro, D., J. de Brito, and L. Evangelista. Evaluation of high-performance concrete with recycled aggregates: Use of densified silica fume as cement replacement. Construction and Building Materials, Vol. 147, 2017, pp. 803-814.
- [47] Shi, C., Y. Li, J. Zhang, W. Li, L. Chong, and Z. Xie. Performance enhancement of recycled concrete aggregate - A review. Journal of Cleaner Production, Vol. 112, 2016, pp. 466-472.

- [48] Liang, C., H. Ma, Y. Pan, Z. Ma, Z. Duan, and Z. He. Chloride permeability and the caused steel corrosion in the concrete with carbonated recycled aggregate. Construction and Building Materials, Vol. 218, 2019, pp. 506-518.
- [49] Chinzorigt, G., M. K. Lim, M. Yu, H. Lee, O. Enkbold, and D. Choi. Strength, shrinkage and creep and durability aspects of concrete including CO<sub>2</sub> treated recycled fine aggregate. Cement and Concrete Research, Vol. 136, 2020, id. 106062.
- [50] Chaofeng, L., F. Yangyan, W. Chunhui, G. Yueqing, and Z. Jiangxia. Damping of rubberized recycled aggregate concrete and damping estimation of its elements by finite element analysis. Composite Structures, Vol. 281, 2022, id. 114967.
- [51] Changging, W., W. Huixia, and L. Chunxiang. Hysteresis and damping properties of steel and polypropylene fiber reinforced recycled aggregate concrete under uniaxial low-cycle loadings. Construction and Building Materials, Vol. 319, 2022, id. 126191.
- [52] Tan, L., X. Jianzhuang, and S. Amardeep. Influence of new-to-old concrete interface on the damping behavior of recycled aggregate concrete. Structural Concrete, Vol. 22, 2021, pp. 3109-3122.
- [53] Chaofeng, L., X. Jianzhuang, W. Chunhui, and M. Zhiming. Hysteretic energy and damping variation of recycled aggregate concrete with different cyclic compression loading levels. Journal of Building Engineering, Vol. 44, 2021, 102936.